MITIGATION AND MODELING SESSIONS

Coupled Biophysical Models of Florida Red Tides

John J. Walsh, Dwight A. Dieterle, Brian P. Darrow, Scott P. Milroy, Jason K. Jolliff, Jason M. Lenes, Robert H. Weisberg, and Ruoying He
College of Marine Science, University of South Florida, 140 Seventh Avenue S, St. Petersburg, FL 33701, USA

Abstract

Coupled three-dimensional models, involving a simple numerical food web of diatoms, toxic dinoflagellates, and microflagellates, regulated by varying CDOM attenuation of light, grown on nitrate, silicate, and ammonium, and gazed by protozoans and copepods, are used to explore the consequences of persistent upwelling of slope water onto the West Florida Shelf during 1998. Diatoms won in both the real world and the model, in the absence of light limitation by CDOM. Yet, a shelf-wide bloom of *Karenia brevis* was simulated in another case of estuarine supplies of CDOM, which allowed successful competition by the model's shade-adapted, poorly grazed dinoflagellates, providing hints about required environmental conditions for red tide initiation.

Introduction

During 1946–1947, a long, pervasive red tide occurred along the West Florida shelf (WFS), which stimulated many ideas on its origin. Two notable ones were that either nitrogen-fixation (Lasker and Smith, 1954) and/or dead fish (Gunther *et al.,* 1948) might be somehow involved as sources of their nutrition, since waters of the WFS were then and still are otherwise oligotrophic today. It also led to the first identification of the ichthyotoxic dinoflagellate as *Gymnodinium breve* (Davis, 1948), now known as *Karenia brevis,* and the first explicit numerical model of their bloom formation, published 50 years ago (Kierstead and Slobodkin, 1953; Slobodkin, 1953). In the process of data analysis of extensive field observations over the last 5 years (Walsh and Steidinger, this Proceedings), with modern high-speed computers and complex three-dimensional simulations in search of sufficient nutrient sources to yield such blooms, we have returned full circle to these early hypotheses in a series of coupled biophysical models of varying complexity of their circulation and ecological components (Penta, 2000; Walsh *et al.,* 2001; 2002; 2003; Darrow *et al.,* 2003; Jolliff *et al.,* 2003; Milroy *et al.,* submitted; Walsh *et al.,* submitted).

Given the limited space, we indulge here in the narcissistic exercise of describing mainly our own results, since numerous references to other work are provided in our previous published studies. We began with a one-dimensional (1-d) model of eight functional groups of phytoplankton, in which a community of small and large diatoms, *Trichodesmium* spp., *K. brevis,* edible dinoflagellates, coccolithophores, autotrophic microflagellates, and coccoid cyanophytes was subjected to different nutrient supplies of estuarine loading and shelf-break upwelling, with background diazotroph excretion in a two-layered physical habitat of constant vertical mixing, described simply by a time-invariant vertical eddy coefficient, k_z (Penta, 2000; Walsh *et al.,* 2001). The other state variables were non-spectral photosynthetically active radiation (PAR), NO_3, NH_4, PO_4, SiO_4, dissolved organic phosphate (DOP), dissolved organic nitrogen (DON), with variable respiration and grazing loss rates of the phytoplankton, but no attenuation of light by CDOM (colored dissolved organic matter) in an attempt to define a minimal numerical niche in which the shade-adapted *K. brevis* would successfully compete against other functional groups of phytoplankton. Different maximal growth rates of the nitrogen-fixer *Trichodesmium* in this first model accounted for their implicit iron-limitation. Vertical migration of *Trichodesmium* and the two groups of dinoflagellates occurred in this model, while settling velocities were a function of cell size.

Results and Discussion

We were able to mimic sparse WFS observations of cell counts of *K. brevis* collected in 1992, 1995, and 1997—as well as during 1976, 1980, and 1986 (Walsh and Steidinger, 2001)—but no assessment of the fidelity of spatial fields could be made in the first 1-d model. Furthermore, 10% of surface PAR can usually be found at a depth of ~30 m on the oligotrophic, subtropical WFS, such that the chlorophyll stocks within the upper 0.5 cm of sediment are usually 2-4 fold those of the overlying water column, until a red tide forms. Accordingly, our second 1-d model retained non-spectral PAR, NO_3, NH_4, PO_4, SiO_4, and diatoms, with addition of a time-dependent k_z, dissolved inorganic carbon (DIC), dissolved organic carbon (DOC), CDOM, nitrifying and ammonifying bacteria, zooplankton fecal pellets, and benthic microalgae (Darrow *et al.,* 2003) to explore pre-bloom conditions of how competitors of *K. brevis* might win in a light-replete but otherwise deleterious nutrient habitat. We now matched the observed demise of the 1996 spring diatom bloom on the WFS, with most of the recycled nutrients utilized by the competing pelagic bacteria and sediment microalgae, whose chlorophyll increment reproduced prior seasonal increases, but no red tide formed in the model's water column, since *K. brevis* was not a state variable (Walsh and Steidinger, 2001).

Our first three-dimensional model of one phytoplankton functional group was next constructed, in which a mature red tide of *K. brevis* was instead subjected to light-cued vertical migration, nocturnal mixing, and wind-driven, time-dependent barotropic transport of a circulation submodel (Blumberg and Mellor, 1987), with k_z computed

Steidinger, K. A., J. H. Landsberg, C. R. Tomas, and G. A. Vargo (Eds.). 2004. Harmful Algae 2002. Florida Fish and Wildlife Conservation Commission, Florida Institute of Oceanography, and Intergovernmental Oceanographic Commission of UNESCO.

during night hours (Walsh *et al.,* 2002). No freshwater runoff, nor internal density structure, *i.e.,* vertical stratification, were considered. Generic nutrient limitation was simulated with different assumed growth rates of *K. brevis,* but light limitation was explicit. Again, PAR was non-spectral, no CDOM was present, and grazing losses were ignored. Given that a red tide was imposed at the beginning of the simulations, the alongshore transport, vertical migration, and landfall of the 1979 and 1980 blooms were indeed now replicated, but the coupled models could not assess the impact of competition, *i.e.,* the onset of red tides, since only one phytoplankton functional group was a state variable, with no explicit pools of nutrients as well.

A second three-dimensional model of three pelagic functional groups thus considered a phytoplankton community of competing diatoms, *K. brevis,* and microflagellates fed slope water supplies of NO_3, NH_4, CO_2, and SiO_4 from a baroclinic version of the same circulation submodel (Weisberg and He, 2003). Note that estuarine and atmospheric sources of nutrients were still ignored to allow easier interpretation of the results of the numerical experiments of this more complex ecological model (Walsh *et al.,* 2003). The circulation model was now forced with winds, freshwater runoff and slope boundary conditions of temperature and salinity, as well as the presence/absence of a Loop Current pressure gradient. With inclusion of vertical stratification, the computed k_z was now a more realistic estimate of vertical mixing, such that nocturnal mixing need no longer be imposed. Other state variables were spectral decomposition of PAR to blue and red light, CDOM as a function of salinity, siliceous fecal pellets of copepods, and non-siliceous ones of protozoans. Benthic remineralization of nutrients was simulated, with bioturbation as a function of the circulation model's near-bottom temperature field, but accumulation of sediment microflora (Darrow *et al.,* 2003) was ignored in this study of the WFS during 1998, when a small fall red tide was instead observed (Walsh and Steidinger, 2001).

The maximal gross growth rates of each phytoplankton functional group of the second 3-d model were also a function of the circulation model's temperature fields (Weisberg and He, 2003). Ammonifying and nitrifying bacteria were now instead implicit variables. Finally, differential grazing, respiration, and settling losses were imposed, with density-dependent mortality of the diatoms. The diatoms won in one case of no light limitation by estuarine CDOM, but lost to *K. brevis* when CDOM was present. In the real world, our field data confirmed that diatoms were indeed the dominant phytoplankton, after massive upwelling in spring of 1998. Yet, the CDOM-free case of the models failed to replicate the observed small red tide in December 1998, tagged with the δN^{15} signature of recycled nitrogen fixation—not that of nitrate-depleted slope waters, and which could then have been fueled by recycled nitrogen of cyanophyte origin (Lenes *et al.,* 2001).

The usual formation of small harmful algal blooms of ~1 μg chl L^{-1} (10^5 cells L^{-1}) in the southern part of the WFS, between Tampa Bay and Charlotte Harbor, must thus instead depend upon local aeolian and estuarine supplies of nutrients and CDOM sun screen, focused at coastal fronts (Steidinger and Haddad, 1991), not those from the shelf-break. Such small red tides have occurred here within nearshore waters 24 out of the last 25 years. In the absence of slope water supplies, local upwelling presumably focuses nitrate-poor innocula of co-occurring *K. brevis* and nitrogen-fixers at coastal fronts for both aggregation and transfer of nutrients between these phytoplankton groups, but with a permutation on the original idea (Lasker and Smith, 1954) that the nitrogen-fixer is *Trichodesmium* spp., not *K. brevis* itself.

In contrast, *K. brevis* is apparently the benefactor, not other phytoplankton (Gunther *et al.,* 1948), from organic nutrient supplies of dead fish, decomposing at the same fronts (Walsh *et al.,* submitted). At red tide levels of ~1×10^5 cells L^{-1} of *K. brevis,* or a biomass of ~1 μg chl L^{-1}, compared to background abundances of 1×10^3 cells L^{-1} in the offshore Gulf of Mexico, fish and manatee kills ensue within nearshore Florida waters, because *K. brevis* is then ichthyotoxic at these higher concentrations (Landsberg, 2002). The dissolved inorganic nitrogen (DIN) source of ~0.4 mmol N L^{-1} for accumulation of just this amount of equivalent phytoplankton nitrogen remains enigmatic, since intrusions of nitrate-rich slope waters yield fast-growing diatom populations, not those of the slow-growing ichthyotoxic dinoflagellate. Nitrogen-fixation by co-occurring *Trichodesmium* and their subsequent release of ammonium, amino acids, and other dissolved organic nitrogen (DON) may instead only fuel the initial population increments of *K. brevis,* since combined local estuarine supplies of dissolved inorganic nitrogen (DIN) and DON from Tampa Bay and Charlotte Harbor meet <5% of the daily nitrogen demand of a small bloom of ~3×10^5 cells L^{-1} (Vargo *et al.,* this Proceedings). Similarly, the results of our third 3-d model (Jolliff *et al.,* 2003) further suggested that photochemical transformation of refractory organic nitrogen to inorganic and labile organic forms within the upstream, far field plume of the Suwannee River on the WFS could have supplied no more than ~5% of the daily nitrogen demand for phytoplankton growth.

As a result of the local P-rich estuaries, more P is added than DIN and DON, but the mean bulk N:P molar ratio of ~48 for most of the 1998–2001 WFS algal communities (Vargo *et al.,* this Proceedings), compared to nutrient-replete culture values of ~15 for *K. brevis,* suggests P-limitation is the ultimate fate of both nitrogen-fixers and red tides. Thus, large blooms of ~1×10^6 cells L^{-1} (10 mg chl L^{-1}) may require an additional source of organic nutrients—a demand of both ~4.0 μmol N L^{-1} and 0.6 μmol P L^{-1} from co-occurring dead fish at convergence fronts, which our recent budgets of the amount of dead fish, their body N and P contents, and their decomposition rates suggest would be sufficient to yield large red tides (Walsh *et al.,* submitted). Again, earlier studies had suggested that the quality of the N/P sources from dead fish was also adequate to maintain

blooms of *K. brevis* (Wilson and Collier, 1955).

We must thus now revise our sequence of the conditional probabilities required for formation of a large red tide of >10 mg chl L^{-1} on the WFS (Walsh and Steidinger, 2001) to include the following: Saharan dust → rainfall → iron-stimulated growth of *Trichodesmium* → their DON release → selective grazing by zooplankton on faster growing dinoflagellate and diatom competitors→ transport by onshore, near-bottom currents of shade-adapted red tide innocula to a P-replete regime for bloom formation at coastal fronts, where *Trichodesmium* and *K. brevis* first are concentrated → initiation of CDOM-shaded *K. brevis* red tide → release of brevetoxins at small red tide levels of >1 μg chl L^{-1} → dead fish, concentrated at the same fronts as those of the co-occurring nitrogen-fixers and *K. brevis* (Gunther *et al.,* 1948), provide the supplement of organic nutrients in a positive feed-back mechanism → red tides of >10 μg chl L^{-1}. To predict the timing and location of the last stage, a WFS model of high fidelity must thus now include physical forcing of a baroclinic model, with time-dependent coastal/offshore boundary conditions of sufficiently fine spatial resolution to allow formation of coastal fronts for aggregation of co-occurring 1) *Trichodesmium* and *K. brevis* from offshore regions of Saharan dust-primed seed populations, 2) CDOM sun-screen, phosphorus, and selective herbivores from nearshore regions of estuarine supplies, and 3) local populations of dead fish, which fortunately can be sensed by aircraft. Reduction of the complexity of this conceptual model requires insertion of surrogate observations to ensure that future operational WFS models of marine "biological weather" do not diverge from the real world at a faster rate than those now used for land prognostications.

Acknowledgements

This analysis was funded by grants NA76RG0463 and NA96OP0084 from the National Oceanic and Atmospheric Administration, N00014-96-1-5024, N00014-99-1-0212, and N00014-98-1-0158 from the Office of Naval Research, R 827085-01-0 from the Environmental Protection Agency, NAG5-6449 from the National Aeronautics and Space Administration, and 1435-0001-30804 from the Minerals Management Service. We also thank the State of Florida for support of these modeling and field efforts.

References

A.F. Blumberg and G. L. Mellor, in: Three-Dimensional Coastal Ocean Models, Vol. 4, N. Heaps, ed. (Washington, D.C.), pp. 208–233 (1987).

B.P. Darrow, J.J. Walsh, G.A. Vargo, R.T. Masserini, K.A. Fanning, and J.-Z. Zhang, Cont. Shelf Res. 23: 1265–1283. (2003)

C.C. Davis, Bot. Gaz. 109:358–360 (1948).

G. Gunther, R.H. Williams, C.C. Davis, and F.G. Smith, Ecol. Monogr. 18:309–324 (1948).

J.K. Jolliff, J.J. Walsh, R. He, R.H. Weisberg, A. Stovall-Leonard, R. Conmy, P.G. Coble, B. Nababan, C. Hu, and F.E. Muller-Karger, Geophys. Res. Lett. 30, doi:10.1029/2003GL016964 (2003).

H. Kierstead and L.B. Slobodkin, J. Mar. Res. 12:141–147 (1953).

R. Lasker and F.G. Smith, Fish. Bull. 89:173–176 (1954).

J.H. Landsberg, Rev. Fish. Sci. 10:113–390 (2002).

J.M. Lenes, B.P. Darrow, C. Cattrall, C. Heil, G.A. Vargo, M. Callahan, R.H. Byrne, J.M. Prospero, D.E. Bates, K.A. Fanning, and J.J. Walsh, Limnol. Oceanogr. 46:1261–1277 (2001).

S.P. Milroy, K.M. Lester, J.J. Walsh, G.J. Kirkpatrick, G.A. Vargo, A. Remsen, R. He, and R.H. Weisberg, Cont. Shelf Res. (submitted)

B. Penta, Ph.D. dissertation, University of South Florida. 1–175 (2000).

L.B. Slobodkin, J. Mar. Res. 12:148–155 (1953).

K.A. Steidinger and K. Haddad. BioScience 31:814–819 (1991).

G.A.Vargo, C.A. Heil, D.N. Ault, M.B. Neely, S. Murasko, J. Havens, K.M. Lester, K. Dixon, R. Merkt, J.J. Walsh, R.H. Weisberg, and K.A. Steidinger, this Proceedings.

J.J. Walsh, and K.A. Steidinger, J. Geophys. Res. 106:11597–11612 (2001).

J.J. Walsh, B. Penta, D.A. Dieterle, and W. P. Bissett, Hum. Ecol. Risk Assess. 7:1369–1383 (2001).

J.J. Walsh, K.D. Haddad, D.A. Dieterle, R.H. Weisberg, Z. Li, H. Yang, F.E. Muller-Karger, C.A. Heil, and W.P Bissett, Cont. Shelf Res. 22:15–38 (2002).

J.J. Walsh, R.H. Weisberg, D.A. Dieterle, R. He, B.P. Darrow, J.K. Jolliff, K.M. Lester, G.A. Vargo, G.J. Kirkpatrick, K.A. Fanning, T.T. Sutton, A.E. Jochens, D.C. Biggs, B. Nababan, C. Hu, and F. E. Muller-Karger, J. Geophys. Res. 108, 3190, doi: 10.1029/2002JC001406 (2003).

J.J. Walsh and K.A. Steidinger, this Proceedings.

J.J. Walsh, G.J. Kirkpatrick, B.P. Darrow, G.A. Vargo, K.A. Fanning, E.B. Peebles, C.A. Heil, J. Havens, and K.A. Steidinger, Cont. Shelf Res. (submitted)

R.H. Weisberg and R. He, J. Geophys. Res. 108, C6, 15, doi:10.1029/2002JC001407 (2003).

W.B. Wilson and A. Collier, Science 121:394–395 (1955).

Effects of Phosphatic Clay Dispersal at Two Divergent Sites in Puget Sound, Washington

J. E. Jack Rensel[1] and Donald M. Anderson[2]
[1]*Rensel Associates Aquatic Science Consultants, 4209 234th St. NE, Arlington, WA 98223, USA;*
[2]*Woods Hole Oceanographic Institution, Biology Department, Woods Hole, MA 02543, USA*

Abstract

Environmental effects of phosphatic clay dispersed inside net pens and removal efficiencies of phytoplankton were evaluated during non-HAB conditions at a well-flushed salmon farm site and at a poorly flushed, nutrient-sensitive inlet remote from any salmon farms. We planned to evaluate the efficacy and effects of *Heterosigma akashiwo* bloom control in large and small pens at a fish farm site, but few cells occurred near the fish farm during our study years, despite low to moderate seasonal concentrations from 1990 to 1999. Experiments were therefore conducted using the normally occurring phytoplankton community. Impervious vertical perimeter skirts, which were open at the bottom, were used alone or installed around pens prior to the tests to initially retain the clay and facilitate study.

Removal efficiencies of microflagellates ranged from 86% to 99%. Prior and post-treatment cell densities were positively related with a correlation coefficient 0.83. Initial dinoflagellate density and removal were low at the salmon farm site but were both much higher for the poorly flushed inlet site. Diatoms dominated at the salmon farm site and were removed at 48% to 87% of the pretreatment density. No significant overall effects on nitrogen (DIN) or phosphorus (PO_4) were observed, although orthophosphate increased inside the pens for short periods after clay application. Turbidity at the surface inside the pens exceeded 100 (large pen) to 500 NTU (small pens) at first and slowly declined. Turbidity at greater depths was typically <50 NTU, probably due to accelerated sinking rates of clay/algal particles. A slight subsurface plume was visible from the surface just outside the large pen, but dissipated rapidly with turbidity similar to background, upstream conditions. The large pen application of 54 kg dry wt. clay resulted in no measurable differences in a series of sediment canisters placed on the bottom in the vicinity of the pen. Percent silt and clay in the top 2 cm of seabottom sediments temporarily increased from 1.7% to 4.2% just downstream of the large pen immediately after the experiment, but additional sampling showed that this type of variability occurs naturally and repeated sampling later indicated no measurable differences. No increase in sediment clay content was noted 30 m downstream at any time. Ten adult salmon placed in the large pen displayed coughing activity after treatment, but recovered quickly as the clay settled.

Introduction

Harmful algal blooms (HABs) are not a major restraint to mariculture worldwide at this time, but they are a continuing problem in some areas (Anderson *et al.,* 2001, Rensel and Whyte 2003). Fish-killing species include a small raphidophyte *Heterosigma akashiwo,* which produces occasional large scale blooms and losses at salmon farms in both northern and southern hemispheres. In the Pacific Northwest, blooms typically occur during mid-summer or early fall in persistently quiescent and warm weather conditions. The last major bloom sufficiently large to kill mariculture fish in Puget Sound was over 10 years ago, but every year some motile cells are observed in the water column. The exact etiology of fish death remains uncertain, but may involve a variety of causes including damage to gills from reactive oxygen species, mucus buildup leading to blood hypoxia or even brevetoxin-like compounds, although the latter has never been definitively documented.

Salmon farmers use a variety of physical mitigation techniques for HABs including water pumping from depth and towing away from blooms. A wide variety of chemicals and treatments have been tried by others to remove or mitigate HABs (Anderson *et al.,* 2001). Collateral damage to other water column or benthic species can be expected from most of these. The use of certain naturally occurring clays to flocculate blooms appears to be effective and have limited environmental impact in some cases. Such clays are used in the western Pacific in Korea, Japan, and China to protect fisheries resources or mariculture, but until recently, environmental studies have been limited. An important consideration for the use of flocculants such as clays involves the possible transfer of algal toxin from the water column to the sea bottom. However, it is most likely that *H. akashiwo* does not produce a persistent toxin, so use of flocculants may be an acceptable means to treat and remove these blooms.

Materials and Methods

Three of the four trials occurred near a commercial fish farm site in Deepwater Bay near Cypress Island in North Puget Sound, during the late summer of 2001. The other trial was conducted in July 2002 in inner most Sinclair Inlet, near Bremerton and Central Puget Sound. The fish farm location is naturally replete with macronutrients and well flushed; the inner reaches of Sinclair Inlet are considered nutrient sensitive (Rensel Associates and PTI Environ. Serv. 1991) and have recurring seasonal microflagellate and dinoflagellate blooms including HABs. Experiment one at the fish farm used a relatively large, 144-m^2 surface net-pen assembly, with nylon nets, impervious, vertical-perimeter skirt to 5 m depth and 10 adult Atlantic salmon inside the pen during the clay application. Experiments 2 to 4 at the fish farm and experiment 5 in Sinclair Inlet utilized a small 4.4-m^2 surface area mesocosm pen consisting only of a

Steidinger, K. A., J. H. Landsberg, C. R. Tomas, and G. A. Vargo (Eds.). 2004. Harmful Algae 2002. Florida Fish and Wildlife Conservation Commission, Florida Institute of Oceanography, and Intergovernmental Oceanographic Commission of UNESCO.

Table 1 Microalgal density in pens (cells/L at 1m) before and after clay treatment and percent removal efficiencies.

	Exp. 1 Large Pen Cypress Is.	Exp. 2 Small Pen Cypress Is.	Exp. 3 Small Pen Cypress Is.	Exp. 4 Small Pen Cypress Is	Exp. 5 Small Pen Sinclair Inlet
Diatoms before	320,000	269,000	446,000	232,000	4,000
Diatoms after	154,000	83,000	106,000	30,000	1,600
Removal Efficiency	52%	69%	76%	87%	60%
Dinoflagellates before	16,000	9,000	8,000	5,000	6,163,000
Dinoflagellates after	16,000	9,000	17,000	7,000	2,005,000
Removal Efficiency	0%	0%	–113%	–40%	67%
Microflagellates before	123,000	60,000	93,000	103,000	846,000
Microflagellates after	17,000	5,000	5,000	6,000	400
Removal Efficiency	86%	92%	95%	94%	99%

nylon perimeter skirt mounted on a frame with 200 g/m^2 loading distributed by a small bilge pump over about 5 minutes. Florida phosphatic clay was hydrated, mixed, screened through 1-mm stainless steel mesh to remove debris and applied via a pressure washer at 375 g/m^2 over 40 min for the large pen trial. Four duplicate sets of 81.1 cm^2 opening area PVC sedimentation collection canisters were placed 5 m upstream and downstream of the large pen at 1, 15 and 30 m distance. Surface and subsurface windowshade drogues and surface floats were deployed during the experiment to confirm the direction and velocity of tidal flow. A petite Ponar grab sampler was used to collect seabottom sediments prior to and after clay treatment and again a week later. The top 2 cm of the undisturbed grab were removed for analysis of sand, silt and clay fractions by screening methods. Sediment samples were not collected in the small pen experiments. Triplicate nutrient, extracted chlorophyll *a*, grain size and solids measurements were according to USEPA-approved protocols. A Hydrolab Surveyor 3 and H20 sonde were used for experiment one. A Hydrolab 4a sonde/surveyor with WET Labs shuttered turbidity probe, Turner SCUFA fluorometer, and other probes was used inside and outside the pens, prior to and during the other experiments. Cell counts were performed using an inverted microscope, with special care as some clay particles were still present in the post-treatment samples. All experiments were conducted during relatively neap tidal periods for about 4 hours, and the large pen experiment began at predicted slack tide based on local NOAA current tables.

Results and Discussion

For Cypress Island experiments, diatoms were the dominant microalgal group, with density ranging from 2.3 to 4.5 × 10^5 c/L (Table 1). Prevalent species in other experiments included *Rhizosolenia setigera* and *Thalassionema nitzschioides.* In other experiments there, *Pseudo-nitzschia* spp., *Skeletonema costatum* and *Thalassionema nitzschioides* were dominant species in varying quantities. Small, unidentified microflagellates (including a few *H. akashiwo*) were numerically significant too, but dinoflagellate density was approximately an order of magnitude less. In Sinclair Inlet, dinoflagellates were much more prevalent, averaging 6.1 × 10^6 c/L prior to treatment and dominated by *Prorocentrum gracile* and *Gymnodinium* spp. Microflagellates were an order of magnitude less abundant, and diatoms were relatively scarce, which is the normal summer condition in this inlet. Microflagellates included unidentified small flagellates, *Platymonas* sp. cf., *Heterosigma akashiwo,* cryptomonads, and choanoflagellates.

Removal efficiencies (RE) of microflagellates after clay use were high, ranging from 86 to 99 percent. The highest efficiency for this group occurred at Sinclair Inlet, which also had the highest initial cell densities. RE of microflagellates was positively correlated to initial cell concentrations for the small pen experiments with a coefficient of 0.83. Lowest RE for this group was in the large pen experiment, which had a protracted period of clay application but higher aerial clay application rate. Diatom RE varied significantly among experiments, from 52% to 87%, with the large pen experiment again having the lowest rate. Dinoflagellate RE was low at Cypress Island (0 to 40%) but much better at Sinclair Inlet where initial densities were 2 orders of magnitudes greater. Collectively, RE was higher for higher initial cell densities, with highest rates for the group of interest, microflagellates. No effect on extracted chlorophyll *a* was noted in experiment 1 or 2, but initial concentrations were very low, only 1.7 and 1.0 µg/L, respectively. Significant reductions were noted in each of the other smaller cage trials where initial concentrations ranged from 4 (Cypress Island) to 15 µg/L at 1 m. The SCUFA *in vivo* chlorophyll *a* results (only collected in Experiments 3–5) generally showed this trend too, but were more variable and suggestive of interferences from the clay despite frequent rinsing of the probe. Water column turbidity prior to treatment at the surface (0.1 to 0.3 m) inside the pens was low to moderate (2 to 5 NTU). Immediately after clay application it rose to >100 NTU for the large pen and ~500 NTU for the small pen, then slowly declined. However, values at depths > 1m did not exceed 50 NTU, probably due to accelerated sinking rates of clay/algal particles at that depth. Turbidity at all depths declined slowly, but remained relatively high near the surface for longer periods. The reason

for this is unknown, but could be related to the generally low initial algal biomass in all but Sinclair Inlet pen. It was possible to see a faint subsurface plume downstream of the large pen, but discrete measurements indicated turbidity levels near background conditions. No plume was seen to escape from the small cages, but tidal currents were minimal.

Sediment grain size nearest the large pen (1 m downstream) showed statistically significant increases of sediment grain size from 1.7% silt/clay to 4.2% silt/clay immediately after the experiment. Subsequent sampling showed naturally large variability in this area and no statistical change from pre-treatment conditions. Current velocity beneath the pens averaged 0.21 m/s during the trial, despite predicted neap tidal conditions. It was unlikely that the clay actually contacted the bottom near the pen, and further downstream (30 m) no significant changes in sediment grain sizes were measured. Sediment collection canister results showed no change from upstream of the large pen to downstream (1, 15 and 30 m). Ten adult salmon placed in the large pen displayed initial coughing symptoms at the outset of that experiment, but recovered quickly as the clay settled. Some of our previous, unpublished work focused on the effects of clay on Atlantic salmon in worst case 5-hour bioassays with constantly resuspended clay treatments of similar loadings. Fish responded by coughing but will cease doing so immediately after removal to clean water. Histopathology of treated fish gills showed no measurable effects from 5 hours of continual exposure.

In summary, these pilot-scale clay treatments demonstrated high removal rates of microflagellates and reasonably good removal of dinoflagellates when initial cell density was great. Careful application of clay treatments will likely not exceed turbidity standards outside permitted mixing zones or result in significant deposition of clay/cell floc immediately downstream of cages. Future studies will report HAB removal results and benthic infauna effects.

Acknowledgements

This effort was supported in part by the U.S. Ecology and Oceanography of Harmful Algal Blooms (ECOHAB) Program sponsored by NOAA, the U.S. EPA, NSF, NASA, and ONR and from in kind contributions of Cypress Island Inc. This is contribution number 10849 from the Woods Hole Oceanographic Institution and Publication 86 of the ECOHAB program. We thank Dr. Rita A. Horner for her careful algal identification and enumeration.

References

D.M. Anderson, P. Andersen, V.M. Bricelj, J.J. Cullen, and J.E. Rensel, Monitoring and Management Strategies for Harmful Algal Blooms in Coastal Waters, APEC #201-MR-01.1, Asia Pacific Economic Program and Intergovernmental Oceanographic Commission Technical Series No. 59, (APEC, Singapore; IOC, Paris) (2001).

Rensel Associates and PTI Environmental Services, Nutrients and Phytoplankton in Puget Sound. US Environmental Protection Agency, Region 10. USEPA Report 910/9-91-002. Seattle. 130 pp. (1991).

J.E. Rensel and J.N.C. Whyte, in: Manual on Harmful Marine Microalgae, G.M. Hallegraeff, D.M. Anderson and A. D. Cembella, eds., IOC Monographs on Oceanographic Methodologies 11 (UNESCO, Paris), pp. 693–722 (2003).

Removal of Harmful Red Tide Plankton by Ozone Treatment

Tsuneo Honjo, Nobuyoshi Imada, Yasuhiro Anraku, Dae-Il Kim, Mikiko Muramatsu, and Yuji Oshima
Dept. Bioscience and Biotechnology, Faculty of Agriculture, Graduate, School, Kyushu University, 6-10-1 Hakozaki, Higashi, Fukuoka 812-8581, Japan

Abstract

We performed research on removing harmful plankton red tides, which involved examining the differences in ozone resistance among 11 phytoplankton species. *Heterosigma akashiwo* and *Chattonella antiqua* cells were all destroyed after 1 min of exposure. The growth of *Prorocentrum minimun, Karenia mikimotoi,* and *Eutreptiella gymnastica* was strongly inhibited after 2 min of exposure. *Cochlodinium polykrikoides* cells decreased to half numbers after 2 min of exposure and died after exposure for 5 min. Growth of *Heterocapsa triquetra* was totally unaffected by 2 min of exposure, but stopped after 5 min exposure. *Heterocapsa circularisquama* had the highest resistance. The growth of *Chaetoceros didymus* and *Ditylum brightwellii* was totally unaffected even by 5 min of exposure, while the growth of *Skeletonema costatum* temporarily decreased after 2 min of exposure, but then steadily recovered. These results imply that ozone treatment is most effective in removing raphidophycean red tides, and is effective in removing harmful algal blooms, except those of *H. circularisquama.*

Introduction

Japan's rapid industrialization, concentration of the population in cities, and lifestyle changes in the 1960s led to the eutrophication of bays and coastal zones, which in turn caused harmful red tides that have taken a heavy toll on the fishing industry (Shirota, 1989a; Honjo, 1994). In recent years, tougher regulations on industrial effluent and residential gray water have decreased the number of red tide occurrences, but damage from new harmful plankton and red tides is still a matter of public concern (Yamamoto and Tanaka, 1990; Matsuyama *et al.,* 1995; Matsuyama *et al.,* 1996). Water quality and bottom sediments must be sufficiently improved to eliminate harm to the fishing industry, but there is still a long way to go before improvements are sufficient to stop red tides. This points to the need to develop a red tide prevention technology that can quickly deal with harmful red tides that harm fishing but will not damage the local marine ecosystem through secondary pollution.

In Japan, red tide prevention technologies now proposed include the spreading of activated clay (Shirota, 1989b), red tide algae-killing bacteria (Sakata, 1990; Imai *et al.,* 1991; Fukami *et al.,* 1992; Imai *et al.,* 1995), viruses (Nagasaki *et al.,* 1999; Tarutani *et al.,* 2001) and titanium oxide with a photocatalytic effect (Matsuo *et al.,* 2001). Spreading activated clay is a practical means, but there are concerns that the clay will eventually accumulate with organic matter in areas with weak currents, and cause bottom sediment deterioration. Red tide algae-killing bacteria and viruses have the advantage that they target only the harmful plankton, but we know too little about their effects on other organisms should the bacteria or viruses mutate. A problem with titanium oxide is that it also kills diatoms, a food source, as well as harmful plankton. If we kill all phytoplankton as titanium oxide does, the local marine ecosystem will be destroyed.

Ozone has an oxidizing capacity second only to that of fluorine, but it soon breaks down into oxygen due to its instability. This research investigated the differences among phytoplankton species regarding their sensitivity to ozone, and examined the changing toxicity of harmful plankton.

Materials and Methods

Test Algae and Culturing Method We isolated *Cochlodinium polykrikoides* from seawater from the Yatsushiro Sea off Kumamoto Prefecture, subcultured every two weeks in Guillard f/2 culture medium (Guillard and Cassie, 1963) without silicate. *Prorocentrum minimum, Karenia mikimotoi, Heterosigma akashiwo, Chaetoceros didymus, Ditylum brightwellii,* and *Eutreptiella gymnastica* were isolated from Hakata Bay, Fukuoka Prefecture, and *Skeletonema costatum* was isolated from the Yatsushiro Sea off Kumamoto Prefecture. The basic culture medium used was modified SWM-III (Itoh and Imai, 1987). All axenic cultures were obtained by pipette purification and cultured aseptically. *Heterocapsa circularisquama* and *Heterocapsa triquetra* were provided by the Fisheries Research Agency's National Research Institute of Fisheries and Environment of Inland Sea, and *Chattonella antiqua* was provided by the Kagoshima University Fisheries Department. Experiments used cells from the exponential growth phase of each culture. The culture was grown and maintained at 25±1°C, 12L:12D, and 100 μmol m^{-2} s^{-1}.

Experimental Method (1) We suspended a suitable amount of each plankton culture in a cylindrical tank (11 cm in diameter, 42 cm high) of filtered seawater and used a Fuji Ozonizer (POX-10) to inject air containing 0.15 mg ozone/L from the bottom of each tank at the rate of 11 L/min. After 0, 1, 2, 5, and 10 min, we took out an amount of the seawater suspension that would contain about 100 cells/mL and used that to inoculate 10 mL of modified SWM-III culture medium (f/2 medium for only *Cochlodinium polykrikoides*) contained in test tubes with screw-on lids (18 mm in diameter, 160 mm high). These tubes were cultured under the above conditions, and cells were counted daily by optical microscopy using a Sedgwick-Rafter count-

Steidinger, K. A., J. H. Landsberg, C. R. Tomas, and G. A. Vargo (Eds.). 2004. Harmful Algae 2002. Florida Fish and Wildlife Conservation Commission, Florida Institute of Oceanography, and Intergovernmental Oceanographic Commission of UNESCO.

Table 1 Effects of ozonation on the removal of various phytoplankton. Symbols in the table represent growth rates (divisions·day^{-1}) of each species.

		Aeration (min)	Ozone exposure time (min)					
Taxon	Species	5	1	2	3	4	5	10
Dinophyceae	*Cochlodinium polykrikoides*	□[a]	□	+++	ND[b]	ND	+++	ND
	Karenia mikimotoi	□	□	+++	ND	ND	+++	ND
	Heterocapsa circularisquama	□	□	++	++	+++	+++	ND
	Heterocapsa triquetra	□	□	++	ND	ND	++	++
	Prorocentrum minimum	□	□	++	ND	ND	+++	+++
Raphidophyceae	*Heterosigma akashiwo*	□	+++	+++	ND	ND	+++	ND
	Chattonella antiqua	□	+++	+++	ND	ND	+++	ND
Eugleophyceae	*Eutreptiella gymnastica*	□	++	+++	ND	ND	+++	+++
Diatomaceae	*Chaetoceros didymus*	□	□	□	ND	ND	□	□
	Ditylum brightwellii	□	□	□	ND	ND	□	ND
	Skeletonema costatum	□	□	□	ND	ND	□	ND

[a]Growth rate : > 0.5 : □, 0.5 ~ 0 : +, 0 ~ –2.0: ++, < –2.0: +++. [b]ND = No Data

ing chamber. The growth rates (divisions · day^{-1}) were determined according to Guillard's formula (1973). At the same time, several cells were also used to inoculate 200 µL of culture medium in a 48-hole multiwell plate (Nunc. Co.), and cell shape was observed daily. As a control, we also injected air at the rate of 11 L/min into plankton seawater suspensions.

(2) We put 600 mL of a suspension of either of two toxic species, *Cochlodinium polykrikoides* (6,500 cells/mL) or of *K. mikimotoi* (3,500 cells/mL) in three 1-L beakers. Into each beaker we put one of a number of longchin goby (*Chasmichthys dolichognathus*) that had been acclimated after their capture off Tsuya Cape in Munakata Country, Fukuoka Prefecture. We observed the plankton shapes and the actions of the fish for 2 h after injecting ozone into each beaker for 0, 1, 2 or 4 min. As a control, we observed the actions of longchin goby in normal filtered seawater without ozone treatment.

Results and Discussion

The effects of ozonation on the removal of various phytoplankton were observed (Table 1). The raphidophyceae *Chattonella antiqua* and *H. akashiwo* had the lowest ozone tolerance of the 11 test species, with all cells rupturing after 1 min of exposure to ozone. The ruptured cells rose to the surface as scum. *Chattonella antiqua*'s fragile cell surface is covered by a thick glycocalyx (Yokote and Honjo, 1985), which controls the electric charge of the membrane surface and functions as receptor of chemical information. For this reason, it is perhaps strongly influenced by oxidation-reduction reactions and is highly sensitive to ozone. *Heterosigma akashiwo,* of the same class, has the same kind of membrane structure (Yokote *et al.,* 1985). The reproduction of *K. mikimotoi* and *P. minimum* was stopped because they did not recover when placed in a new culture medium, although normal-shaped cells were still present after 1 min of exposure. *Cochlodinium polykrikoides* cells were all immobilized after 1 min of exposure, but they retained normal shapes and the next day were reproducing as rapidly as the control group. After 2 min of exposure, the number of cells decreased to about 60%, but in a new medium they recovered their motility after one day. Later their number increased. However, after 5 min of exposure, most of the cells ruptured, leaving a few spherical cells. These spherical cells did not recover even after culturing in a new medium. *Heterocapsa circularisquama* and *H. triquetra,* which have capsules, were immotile spherical cells immediately after 1 and 2 min of exposure. After one day they recovered their motility, and then reproduced. When exposed for 5 and 10 min, the motile and immotile cells in the experimental tank were not observed after three days and one day, respectively. However, the former recovered motility and reproduced six days and seven days after each exposure time. *P. minimum* also has a capsule, but it breaks open with even a slight shock, which is perhaps why it exhibited fragility about the same as that of plankton without capsules. On the other hand, when *H. circularisquama* encounters an unsuitable environment, it survives by breaking out of its capsule and assuming a spherical shape (Honjo *et al.,* 1998; Imada *et al.,* 2001). Therefore, it probably recovered quickly when transferred to a new culture medium because the shorter the exposure time, the less the ozone-induced damage.

Chaetoceros didymus displayed the highest resistance of all the algae tested, suffering no reproductive impediment at all even with 5 min and 10 min of exposure. *Ditylum brightwellii* did not suffer reproductive impediment with 5 min of exposure. This is probably because their tough siliceous capsules do very well at keeping out ozone, thereby reducing cell membrane damage. *S. costatum* reproduction was quite resistant to ozone. After 2 min of exposure, reproduction slowed for a short time, after which the organism resumed propagating as usual.

Our investigation of the toxicity variation of harmful

plankton to longchin gobies showed that the goby in a suspension of *Cochlodinium polykrikoides* was apparently distressed and moved up and down in avoidance maneuvers. One minute of ozone injection made the color of the seawater suspension fade somewhat, but most of the motile cells were observed under a microscope, and the goby continued its avoidance maneuvers. After 2 min of ozone exposure, the seawater's color faded considerably, but while a few motile cells were observed and the fish's avoidance maneuvers decreased, the fish did not behave normally. After 4 min of exposure in the seawater suspension of *Cochlodinium polykrikoides,* the water became colorless with increased consistency, and the cells were not observed at all. The goby placed in this water made no avoidance maneuvers whatsoever. A goby placed in a seawater suspension of *K. mikimotoi* shrank its caudal and pectoral fins, decreased its rate of respiration, and endured its environment by staying motionless at the tank's bottom. One min of ozone exposure faded the water's color considerably, and we saw spherical, immotile cells, but the goby still shrank its caudal fin often and displayed no normal behavior. After 4 min of ozone exposure, the water became colorless, and the goby displayed totally normal behavior. These results show that if ozone is used to eliminate plankton cells, it is also possible to remove toxicity to fish.

Results indicate that ozone treatment is most effective at removing red tides of Raphidophyceae and that it is also effective in removing red tides of some other harmful plankton except for *H. circularisquama.* Schneider and Rodrick (1990) pointed out that a noxious oxidant, hypoboromous acid (HBrO) was formed when ozone was injected in seawater. We hope our studies contribute toward alleviating concerns about effects to marine ecosystems that could result from use of ozone as a practical removal technique for harmful red tide plankton as proposed herein.

References

K. Fukami, A. Yuzawa, T. Nishijima and Y. Hata, Nippon Suisan Gakkaishi 58, 1073–1077 (1992).

R. R. L. Guillard and V. Cassie, Limnol. Oceanogr. 8, 161–165 (1963).

R. R. L. Guillard, in: Handbook of Phycological Methods. Culture Methods and Growth Measurements, J.R.Stein, ed. (Cambridge University Press, Cambridge), pp. 161–165 (1973).

T. Honjo, Rev. Fish. Sci. 2, 225–253 (1994).

T. Honjo, N. Imada, Y. Oshima, Y. Maema, K. Nagai, Y. Matsuyama, T. Uchida, in: Harmful algae, B. Reguera, J. Blanco, M. L. Fernandez and T. Wyatt eds. (Xunta de Galicia and IOC of UNESCO), pp. 224–226 (1998).

N. Imada, T. Honjo, D. I. Kim and Y. Oshima, ITE Lett. 2, 90–93 (2001).

I. Imai, Y. Ishida, S. Sawayama and Y. Hata, Nippon Suisan Gakkaishi 57, 1409 (1991).

I. Imai, Y. Ishida, K. Sakaguchi and Y. Hata, Fish. Sci. 61, 628–636 (1995).

K. Itoh and I. Imai, in: A guide for studies of red tide organisms. The Japan Fisheries Resource Conservation Association, ed., (Shuwa, Tokyo), pp. 122–130 (1987) (in Japanese).

S. Matsuo, Y. Anraku, S. Yamada, T. Honjo, T. Matsuo and H. Wakita, J. Environ. Sci. Health. A36, 1419–1425 (2001).

Y. Matsuyama, K. Nagai, T. Mizuguchi, M. Fujiwara, M. Nishimura, M. Yamaguchi, T. Uchida and T. Honjo, Nippon Suisan Gakkaishi 61, 35–41 (1995).

Y. Matsuyama, K. Nagai, M. Ishimura, M. Yamaguchi, T. Uchida and T. Honjo, in: Harmful and Toxic Algal Blooms, T. Yasumoto, Y. Oshima and Y. Fukuyo eds. (IOC of UNESCO), pp. 247–250 (1996).

K. Nagasaki, K. Tarutani and M. Yamaguchi, Appl. Environ. Microb. 65, 898–902 (1999).

K. Nagasaki, K. Tarutani and M. Yamaguchi, J. Plankton Res. 21, 2219–2226 (2000).

T. Sakata, Nippon Suisan Gakkaishi 56, 1165 (1990).

A. Shirota, Int. J. Aq. Fish. Technol. 1, 25–38 (1989a).

A. Shirota, Int. J. Aq. Fish. Technol. 1, 195–223 (1989b).

K.R. Schneider and G. E. Rodrick, Proc. Trop. Subtrop. Fish. Tech. Soc. Am. 188–192 (1990).

K. Tarutani, K. Nagasaki, S. Itakura and M. Yamaguchi, Aquat. Microb. Ecol. 23, 103–111 (2001).

C. Yamamoto and Y. Tanaka, Bull. Fukuoka Fisheries Mar. Technol. Res. Cent. 16, 43–44 (1990).

M. Yokote and T. Honjo, Exprientia 41, 1143–1145 (1985).

M. Yokote, T. Honjo and M. Asakawa, Mar. Biol. 88, 295–299 (1985).

Pfiesteria piscicida Population Dynamics: A Modeling Study

Xinsheng Zhang, Raleigh R. Hood, Michael R. Roman, Patricia M. Glibert; and Diane K. Stoecker
Horn Point Laboratory, University of Maryland Center for Environmental Science, Cambridge, MD, USA

Abstract

We developed a generalized numerical model to study *Pfiesteria* population dynamics. In addition to modeling the total biomass of *Pfiesteria,* we followed the time dependency of both individual body size and abundance of *Pfiesteria* zoospores. We created model formulations for NON-INDUCIBLE (NON-IND) and TOXIC-A *Pfiesteria* strains by specifying differences in grazing rate, kleptoplastidy, and dissolved organic nitrogen (DON) utilization. We carried out a series of modeling experiments with various sets of model parameter values and attempted to simulate the effects (*e.g.,* turbulence, nutrient concentration and composition, microzooplankton and mesozooplankton (*Acartia*) grazing, and trophic cascade by *Acartia* grazing on microzooplankton) on *Pfiesteria* population dynamics.

Introduction

Pfiesteria piscicida is a mixotrophic, harmful algal bloom species which has a complex life cycle including flagellated, amoeboid, and encysted stages (Burkholder *et al.,* 1995; Burkholder and Glasgow, 1997). *Pfiesteria* has been implicated as the primary causative agent of many fish kills in the coastal waters of the southeastern US. However, the mechanisms that control *Pfiesteria* population dynamics are unclear. Based on our laboratory/field experimental results and literature data, we developed a generalized numerical model to study *Pfiesteria* population dynamics. The model allows us to simulate effects of physical, chemical, and biological conditions and processes on *Pfiesteria* population dynamics. We can use the model outcomes for further testing in the laboratory/field. Therefore, this model provides an important diagnostic tool in the study of *Pfiesteria*.

Model

The model is composed of *Pfiesteria* zoospores, microzooplankton, *Acartia,* dissolved inorganic nitrogen (DIN), DON, diatom, cryptophytes, and detritus (Fig. 1). We used nitrogen as the currency in our model. In addition to modeling the total biomass of *Pfiesteria,* we followed the time dependency of *Pfiesteria* zoospores' cell size and abundance. In this model we represented these two forms of *Pfiesteria* in an idealized way. NON-IND *Pfiesteria* is kleptoplastidic, it does not utilize DON, and it has a relatively fast growth rate. In contrast, TOXIC-A is not kleptoplastidic, it utilizes DON, and it has a slower growth rate. Turbulence is one of the factors controlling the occurrence of *Pfiesteria* blooms (Burkholder and Glasgow, 1997). We derived an empirical function (not shown) of the maximum grazing rate of *Pfiesteria* to turbulence levels and incorporated this factor into the model. According to this equation, *Pfiesteria*'s grazing rate is negatively exponentially related to turbulence levels. This model is an extension of our previous *Pfiesteria* model where we developed an approach for tracking the time dependency of *Pfiesteria* zoospores' cell size and abundance during mixotrophic feeding, and a general, starvation-based mechanism for triggering encystment (Zhang *et al.,* 2003). Most of the formulations and parameter values of this model were based on Zhang *et al.* (2003).

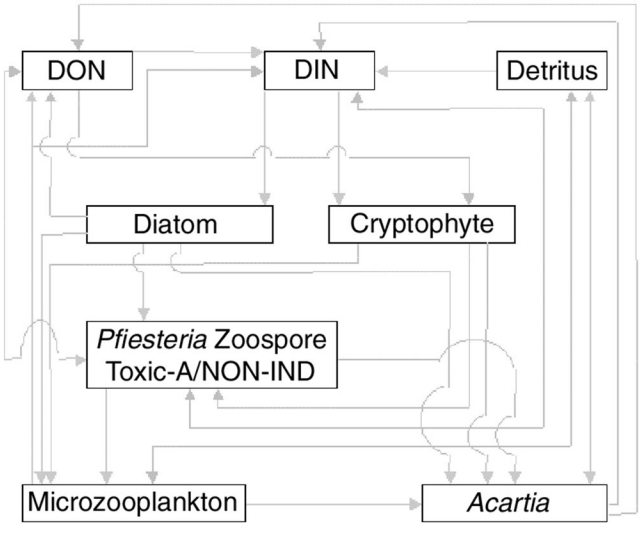

Figure 1 A schematic diagram of the generalized eight-compartment *Pfiesteria* model.

Results and Discussion

Using this generic model, we carried out 6 modeling experiments with a 12-h light and 12-h dark cycle to simulate the effects of 1) turbulence, 2) nutrient concentration and composition, and 3) grazing on both NON-IND and TOXIC-A strains of *Pfiesteria*.

In the first model experiment we compared ecosystem responses in simulations with NON-IND vs. TOXIC-A forms of *Pfiesteria*. In both cases, *Pfiesteria* was subjected to low levels of turbulence and there was no grazing by microzooplankton and *Acartia*. The biomass of diatoms and cryptophytes was depleted quickly by NON-IND *Pfiesteria* (by day 2.5), but zoospore biomass continued to increase due to kleptoplastidy and reached a maximum in day 3.5, then began to decline due to starvation (Fig. 2A); DIN and DON concentrations remained relatively high because the biomass (uptake) of the diatoms and cryptophytes was low (Fig. 2A). In contrast, with TOXIC-A populations the biomass of diatoms and cryptophytes rapidly increased during the first 2 days, reached maxima in day 2, and slowly declined thereafter due to grazing by *Pfiesteria* (Fig. 2B); both DIN and DON concentrations were reduced to low

Steidinger, K. A., J. H. Landsberg, C. R. Tomas, and G. A. Vargo (Eds.). 2004. Harmful Algae 2002. Florida Fish and Wildlife Conservation Commission, Florida Institute of Oceanography, and Intergovernmental Oceanographic Commission of UNESCO.

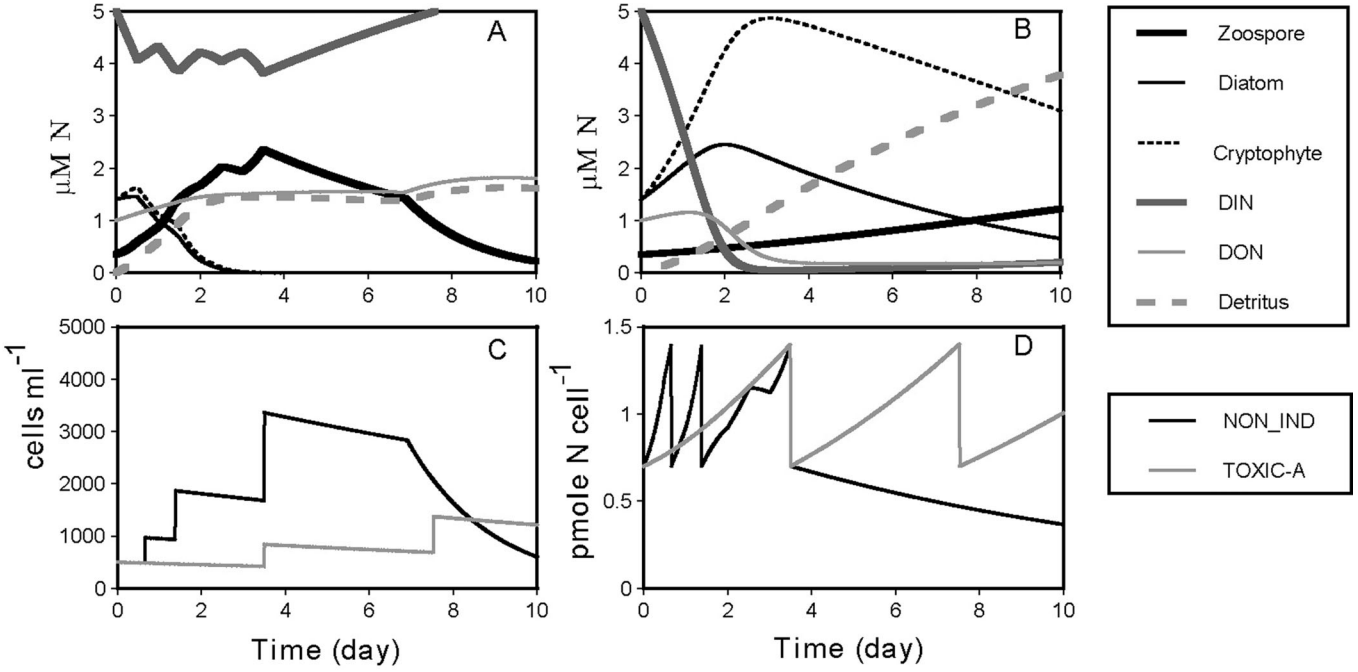

Figure 2 First modeling experiment. *Pfiesteria* zoospore biomass, diatom biomass, cryptophyte biomass, DIN concentration, DON concentration, and detritus concentration vs. time for NON-IND (**A**) and TOXIC-A (**B**). *Pfiesteria* zoospore abundance vs. time (**C**). *Pfiesteria* zoospore size vs. time (**D**).

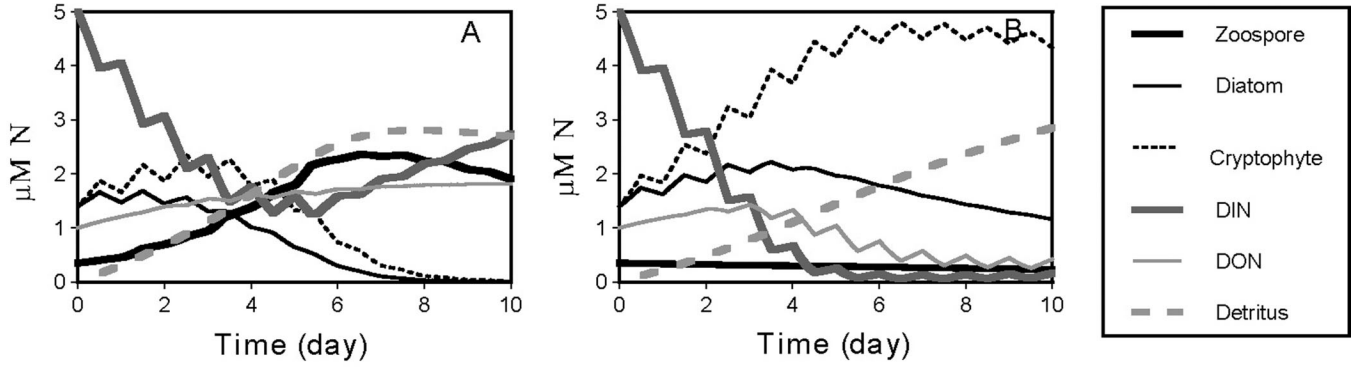

Figure 3 Second modeling experiment. All terms and conditions were the same as in the first experiment except for the higher turbulence. *Pfiesteria* zoospore biomass, diatom biomass, cryptophyte biomass, DIN concentration, DON concentration, and detritus concentration vs. time for NON-IND (**A**) and TOXIC-A (**B**).

levels due to high biomass of diatoms and cryptophytes (Fig. 2B). NON-IND zoospores divided at a faster rate than TOXIC-A cells (Fig. 2C, D). After cell division, the abundance of *Pfiesteria* zoospores doubled (Fig. 2C) and the size of *Pfiesteria* zoospores was reduced to half (Fig. 2D).

In the second experiment, we simulated the effect of increased turbulence on *Pfiesteria* population dynamics. Here, we present only the time dependency of biomass/concentration of each component for the rest of experiments and focus mainly on changes of zoospore biomass. All terms and conditions were the same as in the first experiment except for the higher turbulence. Compared to the first experiment, NON-IND zoospores grew slower and biomass did not reach a maximum until day 7 (Fig. 2A vs. Fig. 3A). TOXIC-A biomass declined throughout the model run (Fig. 2B vs. Fig. 3B). Although turbulence had a negative effect on both NON-IND and TOXIC-A strains, the model results suggest that it is more difficult for TOXIC-A strains to live in high turbulence conditions than for NON-IND strains.

In the third experiment, we simulated the effect of nutrient concentration and composition on *Pfiesteria* population dynamics. All terms and conditions were the same as in the first experiment except for a change of nutrient concentrations from the previously high DIN and low DON condition to a low DIN and high DON condition. Compared to the first experiment, NON-IND zoospore biomass reached a lower maximum in day 3 (Fig. 2A vs. Fig. 4A), and TOXIC-A zoospores grew much faster because more DON was available for utilization/growth (Fig. 2B vs. Fig. 4B).

In the fourth experiment, we introduced the effect of microzooplankton grazing on *Pfiesteria*. All terms and conditions were otherwise the same as in the first experiment. Here, we present only the time dependency of *Pfiesteria* zoospore biomass for the rest of experiments.

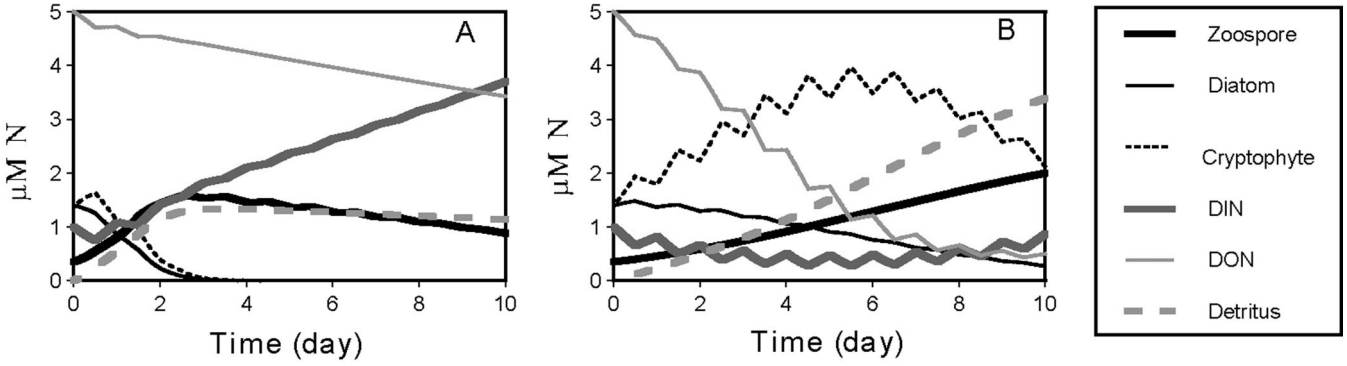

Figure 4 Third modeling experiment. All terms and conditions were the same as in the first experiment except for the change of nutrient condition from the high DIN and low DON to the low DIN and high DON. *Pfiesteria* zoospore biomass, diatom biomass, cryptophyte biomass, DIN concentration, DON concentration, and detritus concentration vs. time for NON-IND (**A**) and TOXIC-A (**B**).

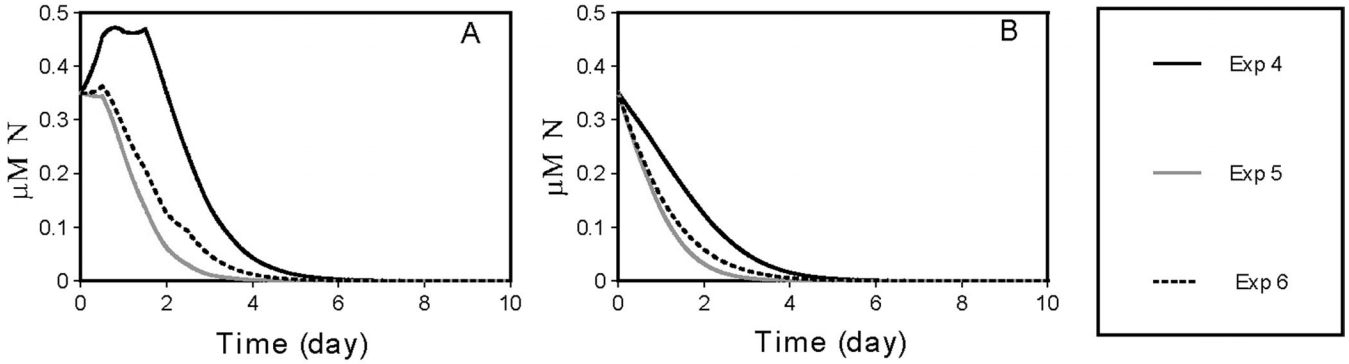

Figure 5 Modeling experiments 4–6. All terms and conditions were the same as in the first experiment except for the addition of microzooplankton grazing (Exp 4), *Acartia* grazing and the assumption that *Acartia* does not eat microzooplankton (Exp 5), deletion of the assumption that *Acartia* does not eat microzooplankton (Exp 6). *Pfiesteria* zoospore biomass versus time for NON-IND (**A**) and TOXIC-A (**B**).

Compared to the first experiment, *Pfiesteria* zoospore biomass declined much faster and was depleted in days 5–6 (Fig. 2 vs. Fig. 5). Therefore, the *Pfiesteria* population in the model was regulated by a combination of bottom-up (food) and top-down (grazing) control.

In the fifth experiment, we simulated the effect of *Acartia* grazing on *Pfiesteria*. All terms and conditions were the same as in the fourth experiment except for the addition of *Acartia* grazing and the assumption that *Acartia* does not eat microzooplankton. Compared to the fourth experiment, *Pfiesteria* zoospore biomass declined even faster and was depleted in days 3–4 (Fig. 2 vs. Fig. 5).

In the sixth experiment, we simulated the effect of trophic cascade; *i.e., Acartia* grazing on microzooplankton which in turn grazes on *Pfiesteria*. All terms and conditions were the same as in the fifth experiment except for removal of the assumption that *Acartia* does not eat microzooplankton. Compared to the fifth experiment, *Pfiesteria* zoospore biomass declined slower and was depleted in days 4–5 (Fig. 2A vs. Fig. 5). Therefore, trophic cascade by *Acartia* grazing on microzooplankton have a positive effect on *Pfiesteria* growth.

Conclusions

In general, the model suggests that the TOXIC-A strain of *Pfiesteria* is more vulnerable to elevated turbulence than NON-IND, but its growth is enhanced by high DON concentrations. Thus, the model predicts that toxic blooms are more likely to occur in calm, organic nutrient-rich conditions, which are often found in shallow, protected tributaries that are subject to anthropogenic effects. These results are generally consistent with observed patterns of toxic blooms in the Chesapeake Bay and the Neuse River of North Carolina (Burkholder and Glasgow, 1997; Glibert *et al.,* 2001).

Acknowledgements

This research was directly supported by NOAA–ECOHAB. This is contribution number 3705 from UMCES.

References

J. M. Burkholder and H. B.Glasgow, Archiv fur Protistenkunde 145: 177–188 (1995).

J. M. Burkholder and H. B.Glasgow, Limnol. Oceanogr. 42(5, part 2): 1052–1075 (1997).

P. M. Glibert, R. Magnien, M. W. Lomas, J. Alexander, C. Fan, E. Haramoto, M. Trice and T. M. Kana, Estuaries 24, 875–833 (2001).

X. Zhang, J. T. Anderson and R. R. Hood, Mar. Ecol. Prog. Ser. 256:29–44 (2003).

Forecasting Red Tides Caused by *Pseudo-nitzschia* spp. Using an Artificial Intelligence Model

J. M. Corchado[2], J. M. Torres[1], and M. M. Sacau Cuadrado[1]
[1]*Departamento de Física Aplicada, Facultad de Ciencias, Universidad de Vigo, Spain;*
[2]*Departamento Informática y Automática, Facultad de Ciencias, Universidad de Salamanca, Spain*

Abstract

This paper presents an artificial intelligence model developed for forecasting *Pseudo-nitzschia* spp. blooms that appear in the coastal waters NW of the Iberian Peninsula. The model is comprised of a Case-Based Reasoning system that incorporates different neural networks for data classification, and identification of similar episodes for forecasting, one week in advance, the quantity of the *Pseudo-nitzschia* spp. that may appear in the Galician coastal area. This model has been used to construct a prototype and the initial results are discussed.

Introduction

Pseudo-nitzschia is a diatom that can produce domoic acid, the toxin responsible for amnesic shellfish poisoning (ASP). Periodic blooms in Galician coastal areas have caused virtual collapse of ecosystems and serious economic impacts. This is a very important reason to develop a model that may help us understand the causes of blooms.

The evolution of these blooms can be seen as a very dynamic system. Forecasting the behavior of a dynamic system is difficult, especially when dealing with poorly known, complex stochastic domains. In this situation, one strategy is to create an adaptive system flexible enough to behave differently depending on the state of the environment. An artificial intelligence (AI) approach to the problem of forecasting in such domains offers advantages over alternative approaches because AI can deal with uncertain, incomplete and even inconsistent data. The AI model discussed is a Case-based Reasoning (CBR) system that incorporates several neural networks and a fuzzy system (FS).

The CBR System for Forecasting

A CBR system solves new problems by adapting solutions that were used to solve previous problems (Corchado and Aiken, 2003; Corchado *et al.,* 2001). The case base holds a number of cases, each of which represents a problem together with its corresponding solution (episode). Once a new problem arises, a possible solution is obtained by retrieving similar cases from the case base and studying their recorded solutions. A CBR system is dynamic in operation because cases representing new problems and their solutions are added, redundant ones are eliminated, and others are created by combining existing cases (Pal *et al.,* 2001).

A CBR system analyses a new problem situation and, by indexing algorithms, retrieves previously stored cases and their solutions by matching them against the new problem situation. It then adapts them to provide a solution to the new problem by reusing knowledge stored in the case base. All of these actions are self-contained and may be represented by a cyclic sequence of processes that may require human interaction. CBR can be an appropriate problem-solving strategy when the knowledge required to formulate a rule-based model of the domain is difficult to obtain, or when the number or complexity of rules relating to the problem domain is too great for conventional knowledge acquisition methods.

A typical CBR system is composed of four sequential steps which are called into action each time a new problem is to be solved (Corchado and Aiken, 2003). These steps are retrieval, reuse, review and retain. The purpose of the retrieval step is to search the case base and select one or more previous cases that most closely match the new problem situation, together with their solutions. The selected cases are reused to generate a solution appropriate to the current problem situation during the reuse (adaptation) stage. This solution is revised (review stage) if necessary, and finally, the new case (*i.e.,* the problem description together with the obtained solution) is stored in the case base.

Cases may be deleted if they are found to produce inaccurate solutions, they may be merged together to create more generalized solutions, and they may be modified over time through the experience gained in producing improved solutions. If an attempt to solve a problem fails and the reason for the failure can be identified, then this information is also stored to avoid the same mistake in the future. This corresponds to a common learning strategy used by humans for problem solving. Rather than creating general relationships between problem descriptors and conclusions, as with rule-based reasoning, or relying on general knowledge of the problem domain, CBR systems can utilize the specific knowledge of previous experience in the form of concrete problem situations.

CBR systems have been successfully used for forecasting in different domains (Corchado and Aiken, 2003; Corchado *et al.,* 2001; Pal *et al.,* 2001). The method requires the use of a numerical method in each of its four reasoning stages. The numerical method used depends on the problem and on the data. The aim of our current work is to develop a system for forecasting *Pseudo-nitzschia* spp. concentrations one week in advance at different geographical locations (E. Fernández,1998) off Galicia. The approach builds on the methods and expertise developed in earlier research (Corchado and Aiken, 2003). The current problem of forecasting may be stated as follows:

- **Given**: a sequence of data values relating to some physical and biological parameters (representative of the current and immediately previous state).

Steidinger, K. A., J. H. Landsberg, C. R. Tomas, and G. A. Vargo (Eds.). 2004. Harmful Algae 2002. Florida Fish and Wildlife Conservation Commission, Florida Institute of Oceanography, and Intergovernmental Oceanographic Commission of UNESCO.

Table 1 Variables that define a case.

Variable	Unit	Week
Date	dd-mm-yyyy	W_{n-1}, W_n
Temperature	°C	W_{n-1}, W_n
Oxygen	mL L^{-1}	W_{n-1}, W_n
pH	acid/base	W_{n-1}, W_n
Transmitance	%	W_{n-1}, W_n
Fluorescence	%	W_{n-1}, W_n
Cloud index	%	W_{n-1}, W_n
Recount of diatoms	cell L^{-1}	W_{n-1}, W_n
Pseudo-nitzschia spp.	cell L^{-1}	W_{n-1}, W_n
Pseudo-nitzschia spp. (future)	cell L^{-1}	W_{n+1}

• **Predict**: the value of a parameter at some future location(s) or time(s).

The raw data (sea temperature, salinity, PH, oxygen and other physical characteristics of the water mass, measured weekly by the monitoring network for toxic proliferations in the Oceanographic Environment Quality Control Center (CCCMM) in Vigo, Spain) consists of a vector of discrete sampled values at 5 m for each oceanographic parameter used in the experiment, in the form of a time series. These data values are complemented by cloud and superficial temperature indexes derived from satellite images, stored with the problem descriptor and subsequently updated during the CBR operation. Table 1 shows the variables that characterize the problem. Data from the previous 2 weeks (W_{n-1}, W_n) was used to forecast the concentration of *Pseudo-nitzschia* spp. one week in the future (W_{n+1}).

A case base was built with this data and the CBR system was constructed using the following techniques, as shown in Table 2:

• The retrieval stage was carried out using a Growing Cell Structures (GCS) ANN (Fritzke,1996) that facilitated indexing of cases and selection of those most similar to the problem descriptor.

• The reuse stage (adaptation of cases) was carried out with a Radial Basis Function (RBF) ANN (Fritzke, 1994) that generated an initial solution, creating a forecasting model with retrieved cases.

• The revision stage was carried out using a group of fuzzy systems (FS) that identify incorrect solutions.

• The learning stage was carried out when the real value of the variable to predict was measured and the error value calculated, updating the knowledge structure of the whole system.

Results and Discussion

The CBR system has been tested along the northwest coast of the Iberian Peninsula with data collected by the CCCMM from the year 1992 until the present time. The prototype used in this experiment was set up to forecast the concentration of *Pseudo-nitzschia* spp. in a water mass situated near the coast of Vigo (geographical area A0 ((42°28.90′ N, 8°57.80′ W) 61 m)), a week in advance. Although the aim of this experiment was to forecast the value of this concentration, the most important thing was to identify in advance if a bloom would form. The average error in the forecast was 26043.66 cells L^{-1} and only 5.5% of the forecasts had an error greater than 100,000 cells L^{-1}. Although the experiment was conducted on a limited data set, we believe the errors are significant enough to be extrapolated over the entire Iberian Peninsula coast.

Two situations of concern are false alarms and undetected blooms. False alarms happen when the model predicts a bloom (*Pseudo-nitzschia* spp. ≥100,000 cells L^{-1}) but one does not occur (real concentration ≤100,000 cells L^{-1}). More important, undetected blooms are when a bloom really exists and the model does not predict one. Table 3 shows successful predictions (in absolute value and %) and erroneous predictions, differentiating undetected blooms and false alarms. This table also shows the average error obtained with other techniques. These results were obtained using cross-validation. The whole data set was divided into 5

Table 2 Summary of technologies employed by the CBR model.

CBR-STAGE	Technology	Input	Output	Process
Retrieval	GCS network	Problem descriptor	k similar cases	All the cases that belong to the same class to which the GCS associates the problem case are retrieved.
Reuse	RBF network	Problem descriptor, *k* similar cases	Initial solution	The RBF network is retrained with the *k* retrieved cases.
Revision	FS	Problem descriptor, Initial solution	Confirmed solution	Different FS are created using the RBF network configuration with different degrees of generalization.
Retain	GCS network, RBF network, FS	Problem descriptor, Forecasting error	Configuration parameters of the GCS network, RBF network and FS	The configurations of the GCS network, the RBF network and the Fuzzy subsystems are updated according to the accuracy of the forecast.

Table 3 Summary of results forecasting *Pseudo-nitzschia* spp., using cross-validation.

Method	OK	OK (%)	Not Detected	False Alarms	Avg. Error (cell L^{-1})
CBR System	191/200	95.5%	8	1	26043.66
RBF	185/200	92.5%	8	7	45654.20
ARIMA	174/200	87.0%	10	16	71918.15
Quadratic Trend	184/200	92.0%	16	0	70354.35
Moving Average	181/200	90.5%	10	9	51969.43
Simple Exp. Smoothing	183/200	91.5%	8	9	41943.26
Brown's Linear Exponential Smoothing	177/200	88.5%	8	15	49038.19

clusters. At times, four clusters were used to create the model and the other was used for testing it. The CBR system was more accurate than any of the other techniques studied during this investigation (see Table 3). This is due to the effectiveness of the revision subsystem and the retraining of the RBF neural network with the cases recovered by GCS network.

The prototype we developed forecasts *Pseudo-nitzschia* spp. with an acceptable degree of accuracy. We believe the results may be successfully extrapolated to forecast even further in the future using the same technique. However, the further ahead the forecast is made, the less accurate the forecast. The prototype can not be used in a particular geographical area if there are no stored cases from that area. Once the system is in operation and forecasting, a succession of cases will be generated, enabling the forecasting mechanism to evolve and work autonomously.

In conclusion, the reasoning problem solving approach can forecast in complex situations where the problem is characterized by a lack of knowledge and where there is a high degree of dynamism. The system will be tested in different water masses and a distributed forecasting system developed, based on the model, to monitor 500 km of the NW Iberian Peninsula coast.

References

J. M. Corchado and J. Aiken,. IEEE SMC Transactions Part C, Nov. 2002, Vol. 32, No. 4, 307–313 (2003).

J. M. Corchado, J. Aiken and N. Rees, Artificial Intelligence Models for Oceanographic Forecasting (Plymouth Marine Laboratory, U.K.) (2001).

E. Fernández, Las Mareas Rojas en las Rías Gallegas, Technical Report, Department of Ecology and Animal Biology, University of Vigo (1998).

B. Fritzke, Neural Proces. Lett., Vol. 1, No. 1, 2–5 (1994).

B. Fritzke, European Symposium on Artificial Neural Networks, ESANN-96, Brussels, 61–72 (1996).

S. K. Pal, T. S. Dilon and D. S. Yeung, Soft Computing in Case Based Reasoning (Springer Verlag: London) (2001).

Preliminary Modeling of Cross-Shelf Transport in Support of Monitoring and Forecasting of Harmful Algal Blooms Along the West Florida Coast

Le Ly[1,2], Frank Aikman III[1], Richard Stumpf[1], and Thomas Gross[1]
[1]*National Ocean Service, NOAA, 1315 E-W Hwy., Silver Spring, MD 20910, USA;*
[2]*On leave from the Naval Postgraduate School, Monterey, CA 93943, USA*

Abstract

In late summer, harmful blooms of *Karenia brevis* routinely occur along the West Florida Shelf and often persist for months. For the past three years, NOAA has had an ongoing effort to monitor and forecast these blooms. Blooms appear to be associated with wind-driven cross-shelf transport, indicating that modeling of this transport may aid in forecasts. A physical-biological coupled model is being developed for harmful algal bloom studies on the West Florida Shelf. The Regional Ocean Modeling System primitive equation model is coupled with simple biological dynamics with four components, NPZD (Nutrient, Phytoplankton, Zooplankton, Detritus). The model has 2.8 km horizontal resolution with realistic bathymetry and 60 vertical terrain-following levels. It has realistic temperature, salinity and wind forcing. The model is initialized with the physical and biological data for late summer (September 2001). Numerical experiments are carried out to study the model physical-biological interactions using wind forcing of September 10–30, 2001, and climatological monthly means (September) of temperature and salinity. The model results are discussed.

Introduction

Some phytoplankters can grow and accumulate into dense, visible patches, often called blooms, near the surface of the water. Many blooms are not harmful, but some phytoplankters produce neurotoxins that can be transferred through the food web where they can affect and even kill invertebrates and vertebrates, including humans. Because phytoplankton contain photosynthetic pigments, large biomass blooms can discolor the surface water where chlorophyll levels can exceed 20 mg chl *a* L^{-1}. Even nontoxic blooms can cause marine mortalities by depleting the oxygen from water and essentially suffocating animals.

Studies have shown that harmful blooms of *Karenia brevis* routinely occur along the West Florida Shelf (WFS) in late summer and often persist for months. These blooms impact fisheries and tourist industries by inducing neurotoxic shellfish poisoning. An effort to monitor and forecast these blooms has been ongoing by NOAA for the past three years. Near-real-time information on likely transport over a week is an important component in forecasting bloom development as part of this effort. Blooms appear to be associated with wind-driven cross-shelf transport, indicating that modeling of this transport may aid in forecasts.

The cross-shelf transport of material properties is closely related with upwelling (or downwelling). The high planktonic productivity is strongly associated with upwelling activities, in which the large-scale upwards vertical velocity, driven by surface winds, provides a supply of nutrients required for phytoplankton photosynthesis in the ocean surface layer. The fundamental effects of physical processes on HABs are (a) to regulate the supply of dissolved inorganic nutrients to the surface layer of the ocean where the phytoplankton must reside to receive and utilize the sun's energy, and (b) to regulate the thickness of the surface-mixed layer, thereby controlling the light levels experienced by phytoplankton. Horizontal variations in biomass, population and HAB structures are increasingly seen to result from horizontal variations in the vertical velocity fields and turbulent structures in the surface-mixed layer. These physical phenomena are closely related to cross-shelf transport and upwelling (or downwelling).

In late summer (September), upwelling-favorable northern to eastern winds often dominate along the West Florida Coast (WFC). Under these conditions, deep cold water is advected shoreward and mixed upward towards the surface, where upwelling is manifested as a decrease in the sea surface temperature. The WFS is gently sloping with a width of around 200 km. Owing to this, the inner shelf is most affected by local wind forcing, and the middle to outer shelf regions are less affected. A physical-biological coupled model is being developed for HAB studies on the WFC. Here, the preliminary modeling effort is presented.

Physical-Biological Coupled Model

The Regional Ocean Modeling System (ROMS) primitive equation ocean circulation model (Song and Haidvogel, 1994) with the full Mellor-Yamada turbulence closure is coupled with a biological model of four components, NPZD (Nutrient-Phytoplankton-Zooplankton-Detritus). The biological model was developed at U.C. Berkeley (Lewis *et al.,* 2001; Edwards *et al.,* 2000). No migration or swimming behavior is included in the biological model, as such behavior is still a subject of great uncertainty. The coupled model, with its realistic bathymetry and realistic wind forcing, is used for September 10–30, 2001. During this period, upwelling-favorable winds from the north, northeast and east dominated the WFC. The model is initialized with monthly mean temperature and salinity forcing, with a 4-day spin-up. The model grid has a size of $302 \times 4 \times 60$ grid points. The model also has 2.8 km uniform horizontal resolution and 60 vertical terrain-following levels to cover an area of 850 km offshore of Sarasota, FL with depths from 10 to 500 m. Since we focus the study on the WFC and WFS, depths greater than 500 m are set equal to 500 m. The physical model is initialized with the monthly mean Global Data Environmental Model (GDEM) temperature (Fig. 1) and salinity for September.

The idealized initial conditions for NPZD include bio-

Steidinger, K. A., J. H. Landsberg, C. R. Tomas, and G. A. Vargo (Eds.). 2004. Harmful Algae 2002. Florida Fish and Wildlife Conservation Commission, Florida Institute of Oceanography, and Intergovernmental Oceanographic Commission of UNESCO.

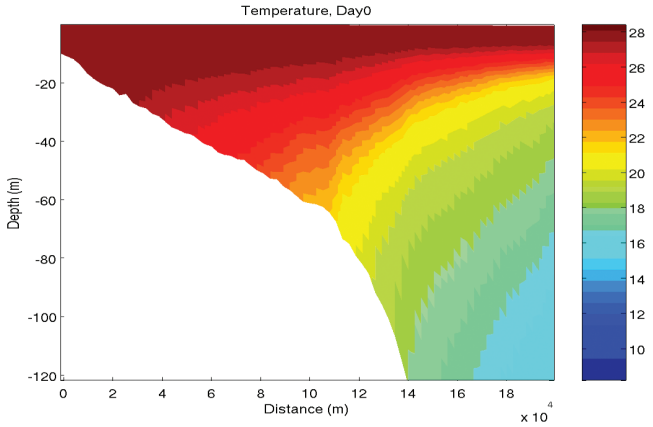

Figure 1 Temperature (°C), Day 0

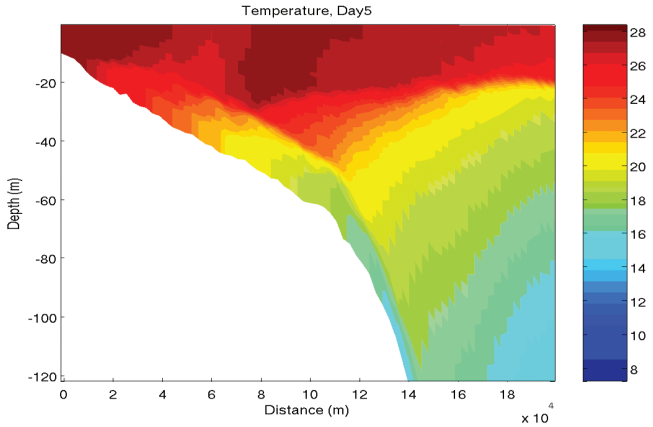

Figure 2 Temperature (°C), Day 5

logical parameters such as nutrient growth rate, grazing, death and remineralization, vertical sinking and other parameters that are given by values in the literature (Tester and Steidinger, 1997; Steidinger *et al.,* 1998; Liu *et al.,* 2001). Light attenuation is given by absorption of water (producing exponential decay with depth). Self-shading is included as an extinction coefficient linearly proportional to the phytoplankton biomass (with specifiable constant). Numerical experiments are carried out to study the model physical-biological interactions when the seawater is vertically stratified (Fig. 1) and using realistic wind time series. This is the condition of the WFS during September 2001.

Numerical Simulations

The model is run for 30 days with a 4-day spin-up on a Silicon Graphics Origin 2000. The simulation results at days 5, 10 and 20 for temperature, nutrients and phytoplankton are presented in Figs. 2–8.

The September initial condition for water is strongly stratified for temperature (Fig. 1) and salinity (not shown). The GDEM September monthly temperature data (Fig. 1) shows temperatures of 26°–28°C in the well-mixed surface layer down to a depth of about 50 m. The primary effect of wind forcing is to advect lighter surface water offshore. Over short time-scales, the response to wind forcing is primarily strong vertical mixing in the near-coastal surface layer out to the 20-m depth contour. The wind forcing for the week-long period (Sept. 10–16, 2001) is persistent over the WFC with speeds of 7 to 15.5 ms^{-1} from the northeast and east directions, producing conditions favorable for upwelling. This wind forcing drives strong upwelling on the WFS. By day 5, the upwelling is well developed (Fig. 2) with the 15°C cold, deep water along the bottom from 120 m depth (140 km offshore) to 40 m depth (60 km onshore).

On longer time-scales, the wind-driven advection moves the buoyant surface water from the near-coast out to 140–150 km offshore (Fig. 4). It is noted that vertical mixing is also strong at this time scale. The upwelling is very strong on day 20 and vertically well-mixed water defines the water column up to 50 m deep and 100 km offshore. At this same time, the cross-shore stratification is evident further offshore and a sharp vertical temperature front is apparent at ~150 km offshore.

The September time series of realistic wind and monthly mean temperature and salinity generate a biological response, which is presented in terms of NP (Nutrient, Phytoplankton) concentrations (μmol N L^{-1}) in Figs. 5–8. The model simulations show that on day 5 (Fig. 5) the upwelling transfers nutrients shoreward along the bottom to the 20-m depth contour, where most of the phytoplankton must reside to receive and utilize the sun's energy. By day 10, the highest nutrient concentrations are found in a layer

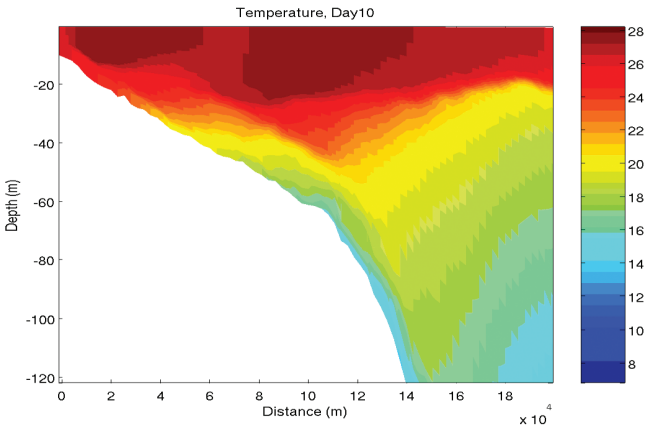

Figure 3 Temperature (°C), Day 10

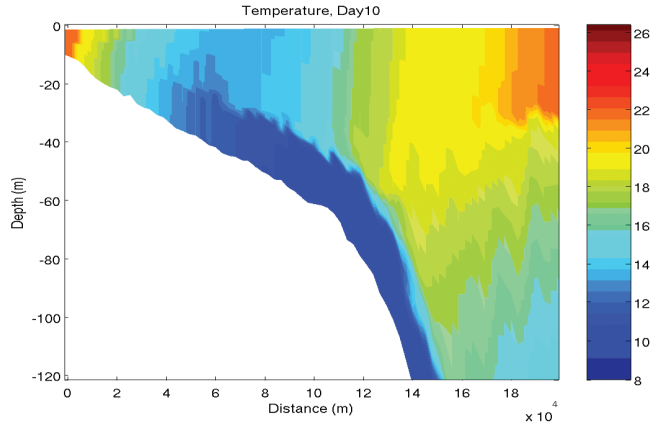

Figure 4 Temperature (°C), Day 20

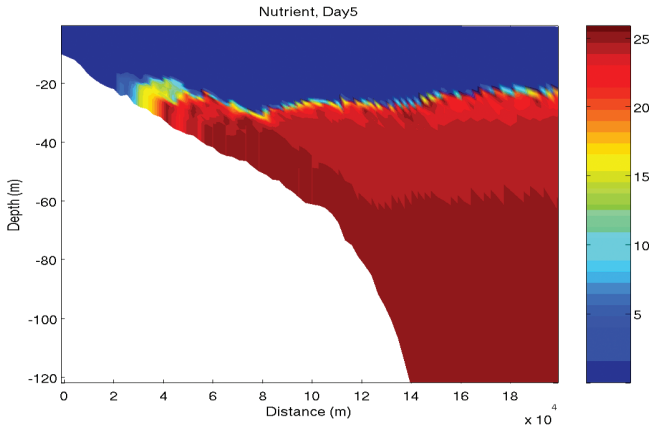

Figure 5 Nutrient (µmol N L^{-1}), Day 5

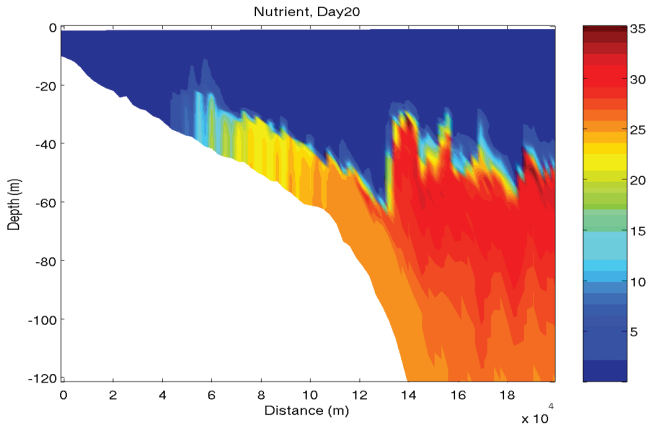

Figure 6 Nutrient (µmol N L^{-1}), Day 20

from 30–60 m depth, along the bottom (not shown). By day 20, the nutrient concentrations have reduced in magnitude, and there is evidence of advection offshore. After day 20, the concentration is not affected by the wind-forced transport, although vertical mixing still has some effect. On day 20, a cross-shore nutrient front is evident at ~140 km offshore (Fig. 6).

The model simulates the effects of wind-forced advective transport on phytoplankton productivity (shallower depths result in higher growth rates in vertically mixed phytoplankton). On day 5 (Fig. 7), the phytoplankton concentration is almost uniform across the shelf in the surface layer of ~20 m depth. Concentrations change rapidly, and by day 10 the highest phytoplankton concentration is located in a layer of ~10 m thickness (at depth of 20–30 m) up to 180 km offshore (not shown). By day 20, wind forcing has advected the phytoplankton offshore, and the phytoplankton concentration is quite well-mixed vertically (Fig. 8).

Conclusion

This work is a preliminary result in developing a physical-biological model applied to the study of HABs on the WFS. The model reproduces some of the basic understanding of the physical and biological conditions on the WFS in September 2001. A strong upwelling event, driven by the surface wind (Sept. 10–30, 2001), provides a supply of nutrients required for phytoplankton photosynthesis in the near-surface layer. Our next step will be to compare the model results with all available remotely sensed and *in situ* observed data.

Acknowledgements

We thank the NOAA National Ocean Service Partnership and MERHAB programs for their support. We would also like to thank Craig Lewis and Thomas Powell of UC Berkeley for their assistance.

References

C.V.W. Lewis, C. Chen, C.S. Davis, Deep-Sea Res. 48, 137–158 (2001).

G. Liu, G.S. Janowitz, D. Kamylowski, Mar. Ecol. Prog. Ser. 213, 12–37 (2001).

C.A. Edwards, T.M. Powell, H.P. Batchelder, J. Mar. Res. 58, 37–60 (2001).

K.A. Steidinger, G.A. Vargo, P.A. Tester, C.R Tomas, in: Physiological Ecology of Harmful Algae Blooms, D.M. Anderson, A.D. Cembella and G.M. Hallegraeff, eds. (Springer-Verlag, New York) (1998).

P.A. Tester and K.A. Steidinger, Limnol. Oceanogr. 42, 1039–1051 (1997).

J.T. Turner and P.A. Tester, Limnol. Oceanogr. 43, 1203–1214 (1997).

Y.T. Song and D.B. Haidvogel, J. Comput. Phys. 115, 228–244 (1994).

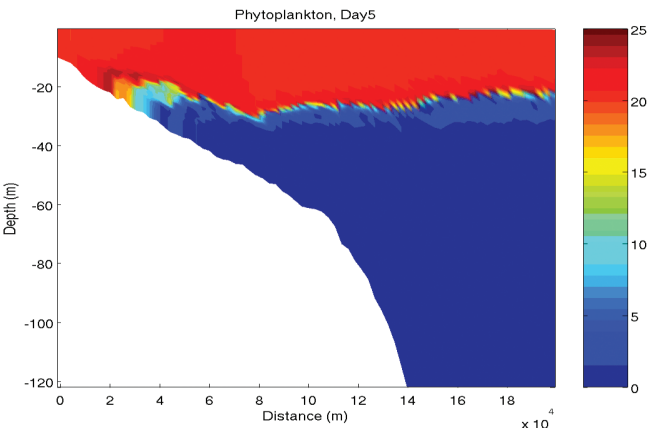

Figure 7 Phytoplankton (µmol N L^{-1}), Day 5

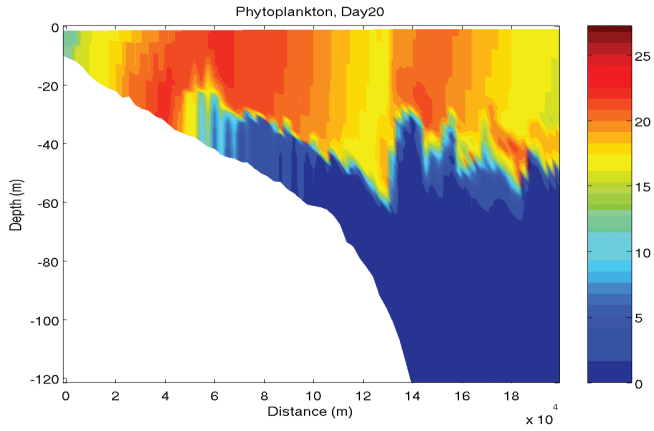

Figure 8 Phytoplankton (µmol N L^{-1}), Day 20